# Robust Angle-Sensorless Control of a PMSM Bearingless Pump

Klaus Raggl, *Member, IEEE*, Bernhard Warberger, Thomas Nussbaumer, *Member, IEEE*, Simon Burger, and Johann W. Kolar, *Senior Member, IEEE*

***Abstract*—In the semiconductor industry, where bearingless pump systems are employed as the state-of-the-art technology, the trend goes toward higher fluid temperatures (150 °C and more) in order to further increase process efficiency. This fact translates into the requirement of a high-temperature bearingless pump system and/or the elimination of thermal-critical components such as Hall sensors. This paper introduces a new method for a hall-sensorless control of a permanent-magnet synchronous machine bearingless pump in its operating range from 0 to 8000 r/min and from zero load to full load. The sensorless operation is performed by the following three novel control functionalities: a controlled startup routine, enabling a sure levitation and zero-angle setting; an open-loop angle estimation based on stator voltage and stator current measurement and known machine parameters; and an angle synchronization establishing a robust operation of the pump in the whole operating range even for a large machine parameter drift. In particular, considering the temperature degrading of the permanent-magnet flux density, the novel robust control concept is of great benefit for bearingless pump systems employed in high-temperature applications.**

***Index Terms*—Angle synchronization, bearingless pump, permanent-magnet synchronous machine (PMSM), sensorless control.**

## I. Introduction

BEARINGLESS motors have been extensively investigated in the past and have been employed successfully in high-purity environments (e.g., in semiconductor, pharmaceutical, and medical industry) due to their great variety of benefits such as noncontact bearing capability and the lack of mechanical wearing, lubricants, and seals [1]–[4]. In addition, they feature high power density; thus, these pumps are, nowadays, the best choice for high-purity and high-tech areas, e.g., in semiconductor process applications. In order to further increase the productivity and process quality, higher temperatures of the process fluids are employed more and more.

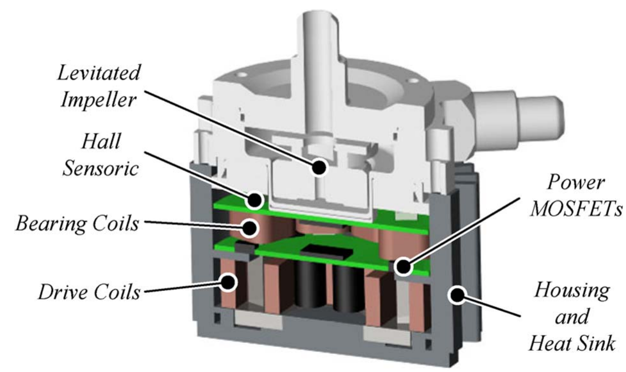


Fig. 1. Sectional view of a bearingless pump system with fully integrated power electronics.

These high fluid temperatures cause problems for the bearingless pump system. Fig. 1 shows the sectional view of a bearingless pump system with integrated power electronics [5]. As one can see, the sensors for detecting the radial and angle positions have to be positioned close to the impeller in order to measure satisfying signals. Particularly for the angular Hall sensors, the vicinity to the high-temperature fluid is very critical, which raises the demand for a sensorless control of the bearingless pump, i.e., the complete elimination of the Hall sensors. The radial position sensors can be assembled based on inductive or eddy-current principle and are therefore not thermally critical.

In the literature, many methods for eliminating angle and speed sensors have been established [6]–[8]. The motivation in most cases was to eliminate the sensors for reasons such as costs, reliability, weight, and size of the machine. However, for the considered high-tech applications, such cost-related aspects are of minor importance compared to the technological challenge associated with the high-temperature application.

In contrast to most concepts presented in the literature, which are typically built up as three-phase motors driven by three-phase half-bridge modules, the existing bearingless pump is built up with a two-phase drive system, which is driven by two full bridges. The reason for this choice is the combination of the bearing and drive together on one iron circuit [1]–[3]. The established concepts in literature can be subdivided into methods using the induced voltage $u_{\mathrm{ind}}$ [9]–[15] on one hand and methods measuring the rotor-angle-dependent phase inductance on the other hand [16]–[18]. However, the back-EMF methods are not useful at low speed and standstill, and the

Manuscript received December 19, 2007; revised January 29, 2008. First published February 10, 2009; current version published June 3, 2009.

K. Raggl was with the Power Electronic Systems Laboratory, Swiss Federal Institute of Technology (ETH), 8092 Zurich, Switzerland. He is now with Hilti AG, 9494 Schaan, Liechtenstein (e-mail: klaus.raggl@hilti.com).

B. Warberger was with the Department for Electrical Drives and Power Electronics, Johannes Kepler University Linz, 4040 Linz, Austria. He is now with Levitronix GmbH, 8005 Zurich, Switzerland.

T. Nussbaumer was with the Power Electronic Systems Laboratory, Swiss Federal Institute of Technology (ETH), 8092 Zurich, Switzerland. He is now with Levitronix GmbH, 8005 Zurich, Switzerland.

S. Burger was with the Power Electronic Systems Laboratory, Swiss Federal Institute of Technology (ETH), 8092 Zurich, Switzerland. He is now with Speck Pumpen GmbH & Co. KG, 91233 Neunkirchen am Sand, Germany.

J. W. Kolar is with the Power Electronic Systems Laboratory, Swiss Federal Institute of Technology (ETH), 8092 Zurich, Switzerland.

Color versions of one or more of the figures in this paper are available online at http://ieeexplore.ieee.org.

Digital Object Identifier 10.1109/TIE.2009.2014745

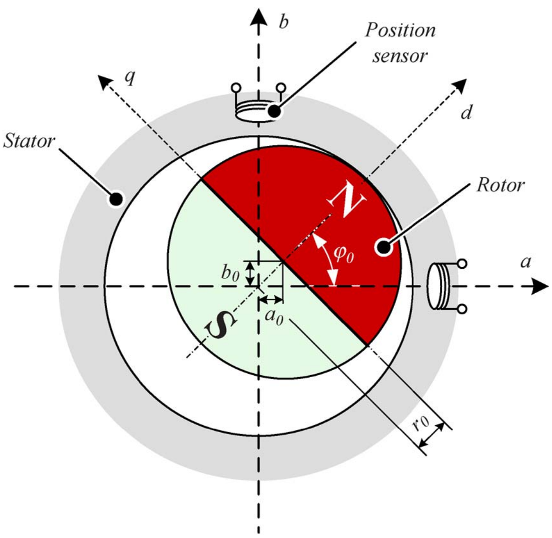


Fig. 2. Rotor position at standstill and start angle calculation.

phase-inductance measurement is not effectual at high speed. For the high-temperature bearingless pump system, the rotor angle is needed from standstill to ensure levitation until high speed of approximately 8000 r/min to achieve the needed output power.

In the following, methods for estimating and calculating the rotor angle without using any Hall sensors will be described. Section II introduces a method to calculate the initial rotor position at standstill, since this angle is very important to ensure levitation and a proper angle estimation. In Section III, a simple method for estimating the rotor angle out of the phase voltages, currents, and given machine parameters is introduced. Finally, a new method for synchronizing the estimated rotor angle by measuring the freewheeling current in one drive phase will be introduced in Section IV. The improvement of the synchronization method regarding robustness against dynamic load and rotational speed changes will be shown in Section V by measurements on an existing pump system. In addition, measurements verify the correctness of the theoretical considerations in each section.

## II. Startup Routine

Starting up levitation without the knowledge of the rotor-angle position is an inherent challenge of bearingless pumps, since the rotor angle is needed to apply the superposed magnetic field for suspension force generation. A detailed force generation description can be found in [19].

First of all, the initial rotor angle has to be found. For the estimation of the rotation angle at standstill, several possibilities for bearingless motors are well known (see, e.g., [20]). The goal is to estimate the initial angle position without turning the rotor, which would cause abrasion. The biggest advantage of bearingless pump systems is the contact-free handling and, hence, a low contamination of the pump medium.

The needed initial rotor angle $\varphi_0$ can be found by using an inherent property of unipolar permanent magnets: Looking at Fig. 2, one can see that the rotor is always sticking to the stator wall with one magnet pole but not being defined as to which

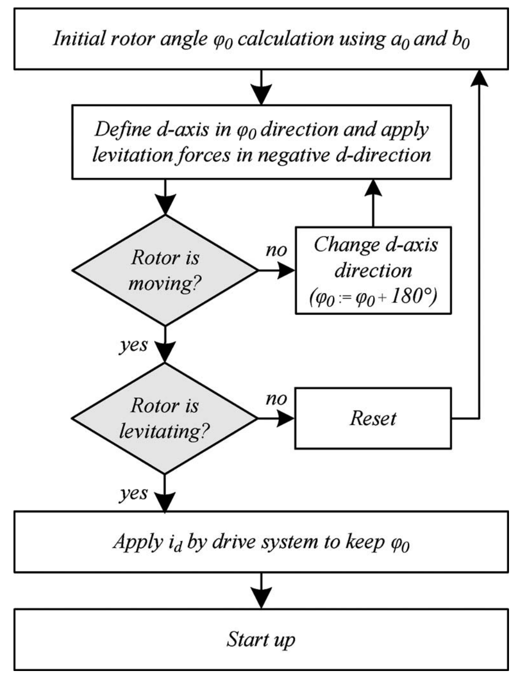


Fig. 3. Startup algorithm flow diagram.

one. However, it is not assured that the orientation of the magnet is exactly according to its polarization, i.e., the point of contact is not exactly the magnet pole. First, this is due to reluctance forces to the stator claws which are placed at some defined positions of the stator. Second, it is not sure which pole (south or north) is directed to the wall. The initial rotor angle $\varphi_0$ can now be assumed using the included radial position sensors for $a$- and $b$-axes

$$\varphi_0 = \arctan\left(\frac{b_0}{a_0}\right). \tag{1}$$

For starting up levitation, the algorithm shown in Fig. 3 can be used. After having set the initial rotor angle out of (1), the correct magnet pole has to be found. Since the rotor can stick either with the north pole or with the south pole at the stator wall, the initial rotor angle can be assumed wrongly by 180°. In the used algorithm, the north pole is assumed to point toward the stator wall first. Afterward, a rotor fixed frame ($d$- and $q$-axes) is defined by setting the $d$-axis in the direction of $\varphi_0$. Activating now the levitation will lead to forces in negative $d$-axis and a resulting rotor displacement.

This displacement depends on the magnet direction in reality. If the north pole was sticking, the assumption was right and the rotor will move toward the stator center. In contrast, if the south pole is directed toward the stator wall, the initial rotor angle $\varphi_0$ was calculated wrongly by 180° and has to be corrected. One might think that the displacement, which is necessary to detect which pole is sticking at the stator wall, can be calculated out of the relative change of $r = r_0 \pm \Delta r$ (with $\Delta r = \sqrt{\Delta a^2 + \Delta b^2}$). However, this calculation may fail, since a radius decrease (which would mean a sticking north pole) can also be detected for a small rotation of the rotor with the south pole sticking at the stator wall. The reason for this is the nonlinear characteristic of the position sensorics together with the circular shape of the

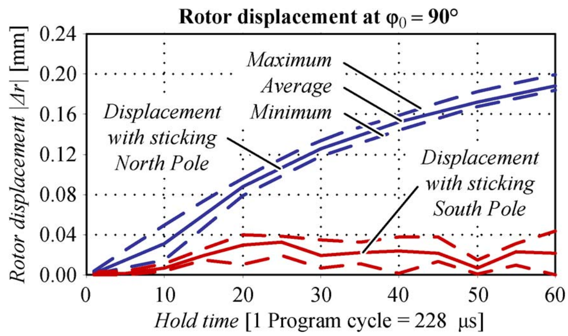


Fig. 4. Rotor displacement in dependence on time and which pole is sticking to the stator wall.

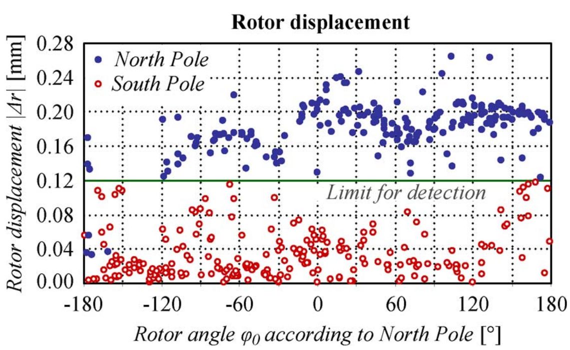


Fig. 5. Rotor displacement in dependence on the rotor angle $\varphi_0$ and which pole is sticking to the stator wall for a wait time of 50 program cycles (11.4 ms).

rotor surface. Since the algorithm is still expecting the rotor north pole sticking, the reference bearing current will increase constantly due to the PID position controller. Thus, this may lead to an overcurrent situation caused by the subordinate PI current controller.

Therefore, the absolute radius change $r = |\Delta r|$, instead of the relative radius change, is used to identify the sticking pole. Measurements done with this estimation are shown in Fig. 4. One can see that the radius change in case of a sticking south pole reaches lower values in comparison to the radius change in case of a sticking north pole. After a short hold time of approximately 50 program cycles, which is equal to 11.4 ms, the difference between both lines is big enough to determine the sticking pole. On the other hand, this time is short enough to ensure that in case of the south pole sticking at the stator wall, no damage of the bearing coils will appear due to the current impressed into the coils.

In Fig. 5, the dependence of the rotor displacement after a hold time of 11.4 ms on the rotor angle is shown for various cases of north and south poles sticking at the stator wall, respectively. One can see that for most of the 200 measurements, the radius displacement is different between sticking north or south pole, and a limit to decide which pole is sticking can be found. Although most of the points are far below or beyond the limit, it may appear that the sticking pole is not detected correctly. Thus, the rotor is not levitating after a defined waiting time, which will lead to a reset by the algorithm shown in Fig. 3, and the startup operation will be started again until the correct pole orientation is detected.

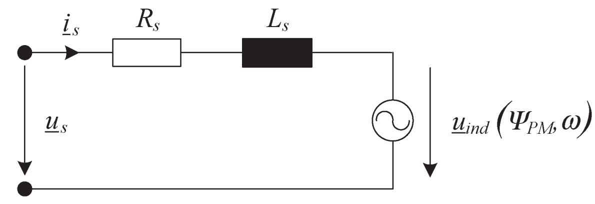


Fig. 6. Equivalent circuit diagram of a common PM synchronous motor drive.

Once the pole detection succeeded, the rotor starts to levitate. It is important to keep the initial rotor angle $\varphi_0$, since this angle is needed for the further angle calculation. Therefore, a current $i_d$ is applied by the drive system to fix the rotor (cf. Fig. 3).

After starting the rotor up to levitation, it can now be accelerated up to the minimum needed speed to turn on the sensorless position estimation, by rotating $i_d$ impressed by the drive system in a feedforward operation. The switch between feedforward acceleration and sensorless control has to be done at a rotational speed, where virtually no mechanical load appears. Since a typical operation point of the used magnetically levitated pump is beyond 4000 r/min, turning on the sensorless operation is possible in between the speed ranges of 1000 and 4000 r/min. As it will be shown in the forthcoming section, the minimum needed speed to ensure a proper angle calculation is in the range of 1000 r/min. Therefore, the rotor is accelerated up to 1000 r/min and a switch to the sensorless operation can be performed there without losing information about $\varphi_0$.

## III. Rotor-Angle Estimation

In this section, a simple but effective rotor-angle-estimation method will be described. The principle is based on the estimation of the back-EMF-induced voltage $u_{\text{ind}}$ by using the knowledge of the stator voltage $u_s$ and calculating the load angle $\gamma$ between the stator voltage $u_s$ and $u_{\text{ind}}$ [21]. Fig. 6 shows the equivalent circuit of a standard permanent-magnet synchronous machine (PMSM). Out of this, the vector diagram for field-oriented control [shown in Fig. 7(a)] can be drawn. To ensure field-oriented control and therefore highest available motor power, the actual rotation angle $\varphi$ has to be known. This angle appears between the rotor fixed $d-q$ system and the stator fixed $a-b$ frame.

The goal is to estimate the position of the rotor fixed $d$-axis, respectively, the angle $\varphi$, out of known values like the impressed stator currents or voltages. The stator voltage

$$\underline{u}_s = \begin{bmatrix} U_{s,a} \\ U_{s,b} \end{bmatrix} \tag{2}$$

can be used to calculate the voltage angle $\alpha$ [22]

$$\alpha = \arctan \frac{U_{s,b}}{U_{s,a}}. \tag{3}$$

Without any mechanical load, the stator voltage $\underline{u}_s$ is in phase with the induced voltage $\underline{u}_{\text{ind}}$. By applying a mechanical load, an additional angle $\gamma$ between the stator voltage $\underline{u}_s$ and the induced voltage $\underline{u}_{\text{ind}}$ appears. This load-specific angle can be calculated for a certain angular frequency $\omega$ using the machine

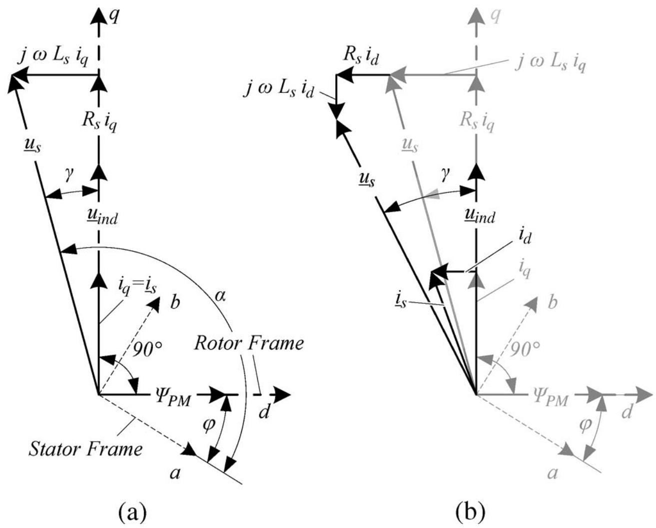


Fig. 7. Vector diagram of a common PM synchronous motor with (a) field-oriented control, out of (b) field-oriented frame.

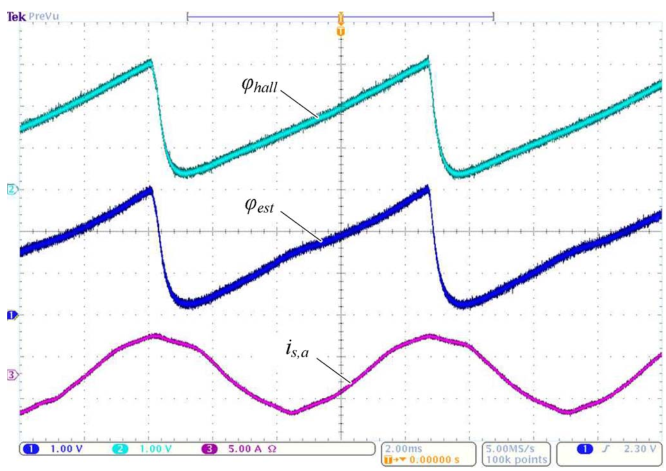


Fig. 8. Angle calculation at 7000 r/min in comparison to measured angle at a hydraulic operation point of 6.5-L/min hydraulic flow and 1.3-bar outlet pressure (angle scale: 120°/div; current scale: 5 A/div; and time scale: 2 ms/div).

parameters $L_s$, $R_s$, and $\Psi_{\mathrm{PM}}$ and the phase current $\underline{i}_s$ or in case of field-oriented control $i_q$

$$\gamma = \arctan \frac{\omega i_q L_s}{i_q R_s + \omega \Psi_{\mathrm{PM}}}. \tag{4}$$

In case of small resistance values $R_s$, a speed-independent load angle results in

$$\gamma = \arctan \frac{i_q L_s}{\Psi_{\mathrm{PM}}}. \tag{5}$$

All needed values to calculate $\alpha$ and $\gamma$ (stator phase voltages $U_{s,a}$, $U_{s,b}$, the stator current $i_q$, and the machine parameters $L_s$ and $\Psi_{\mathrm{PM}}$) are known, and the estimated rotor frame angle $\varphi_{\mathrm{est}}$ can be calculated to

$$\varphi_{\mathrm{est}} = \alpha - \gamma - 90°. \tag{6}$$

Measurements, as shown in Fig. 8, show that the actual (upper line) and the estimated (middle line) rotor angle match very well, i.e., the load angle $\gamma$ is estimated correctly.[1] For the measurements, a test setup (cf. Fig. 9) consisting of the bearingless pump, a hydraulic tank, water pipes, pressure and flow sensors, and a ball valve to change the hydraulic load was used.

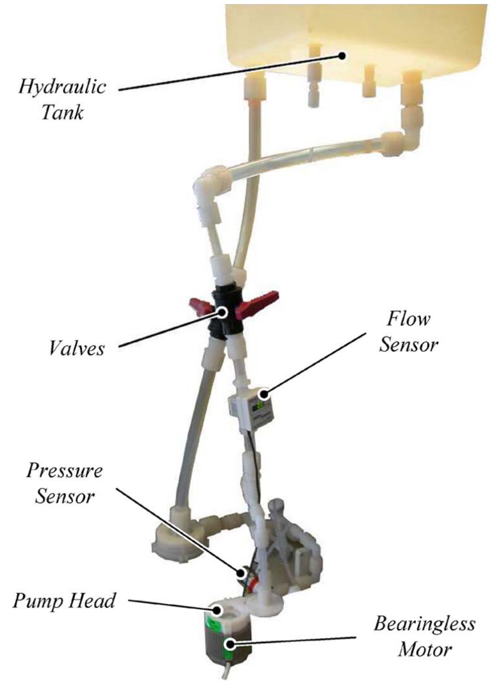


Fig. 9. Test setup of the bearingless pump system.

The minimum achievable speed with this method depends mainly on the minimum stator voltage needed for a sufficiently exact calculation of (3), i.e., at low speed, the amplitude of $\underline{u}_s$ is too small to calculate $\alpha$ correctly. The minimum achievable speed for the pump at hand has been identified with 1000 r/min.

The introduced angle-estimation method works satisfactory if the machine parameters $L_s$ and $\Psi_{\mathrm{PM}}$ are well known. However, uncertainties in these values lead to a computational error in (4). This results in a wrong rotor angle $\varphi$ and, hence, in an incorrectly impressed stator current $\underline{i}_s$. The consequence is a resulting current component $i_d$ as shown in Fig. 7(b). The additional current $i_d$ leads to a voltage drop $R_s i_d$ and $\omega L_s i_d$ and, consequently, to an increased stator current $\underline{i}_s$. In practice, this means more needed current to drive the motor and, thus, a decreased maximum power and efficiency of the drive system.

In the same manner, also an error in calculating $\varphi_0$ during the startup sequence leads to a constant angle error in (6). In order to avoid parameter and initial angle dependence, it is indispensable to synchronize the rotor angle from time to time with a real physical parameter. In the following section, an effective synchronization by means of freewheeling current will be presented.

[1]The actual angle $\varphi_{\mathrm{hall}}$ is measured for comparison reasons in a conventional manner through two reference Hall sensors $H_x$ and $H_y$ by evaluation of $\arctan(H_y/H_x)$ inside the DSP. Due to the limited number of output ports, both angle signals $\varphi_{\mathrm{hall}}$ and $\varphi_{\mathrm{est}}$ could only be displayed through the PWM output ports and a subsequent low-pass filter, which is the reason for the round shape of the angle signals at the falling edges.

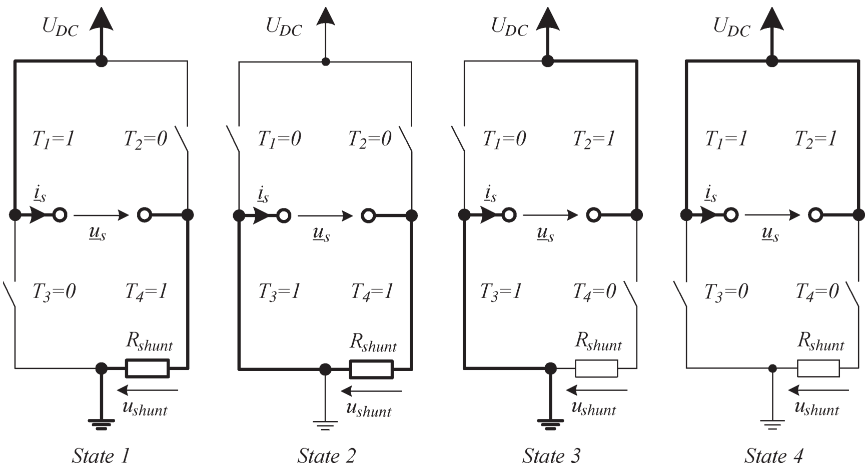


Fig. 10. Switching states within one pulse period for an inverter bridge of one drive phase using three-level PWM. State 1: positive inductor voltage. State 2: freewheeling path, current in the inductor is decreasing. State 3: negative inductor voltage. State 4: freewheeling path, decreasing inductor current.

In addition, due to the fact that the introduced method is only a feedforward control, a potential failure of the angle estimation and/or speed calculation and even a system crash cannot be detected by the control, which incorporates a drawback for practical implementation.

## IV. Rotor-Angle Synchronization by Freewheeling Current Measurement

Driving a motor only with rotor-angle estimation may lead to a wrongly calculated angle due to uncertainties in the parameters and, thus, to a non-field-oriented operation as described before. The angle estimation is basically a feedforward control with a correction of the load-dependent angle offset between the stator voltage $\underline{u}_s$ and the induced voltage $\underline{u}_{\text{ind}}$. Therefore, in this section, a method is described, how the wrongly calculated rotor angle can be detected and synchronized by measuring the physical rotor position using the freewheeling current.

Fig. 10 shows the four appearing switching states within one pulse period for a full bridge driven by a three-level PWM signal. To achieve a lower current ripple in the motor inductor, the voltage over the inductor is set to zero for two switching states (states 2 and 4). During state 2, the impressed inductor current is flowing through the freewheeling path and through the current measurement, which can be realized as a simple shunt resistor.

If the freewheeling state (state 2) is applied for a longer time period (several milliseconds), the current waveforms shown in Fig. 11 appear. State 2 is active from $\varphi_{\text{off}}$ until $\varphi_{\text{on}}$. The current $i_s(t)$ measured by the current sensor is, in general, a superposition of two fictitious currents

$$i_s(t) = i_{s,f}(t) + i_{\text{ind},f}(t) \tag{7}$$

which occur due to the superposition of two voltage sources, namely, the stator voltage $u_s(t)$

$$u_s(t) = U_s \cdot \sin(\omega t + \gamma) \tag{8}$$

with

$$U_s = \sqrt{(\omega \Psi_{\text{PM}} + i_q R_s)^2 + (i_q \omega L_s)^2} \tag{9}$$

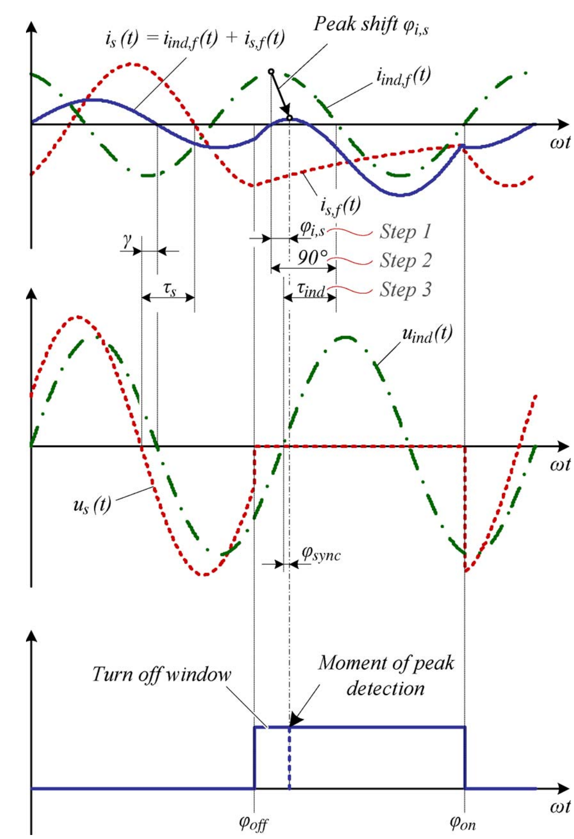


Fig. 11. Superposition of fictitious phase currents and peak detection during the turn-off window.

for field-oriented control $(\underline{i}_s = i_q)$ and the induced voltage $u_{\text{ind}}(t)$

$$u_{\text{ind}}(t) = \omega \Psi_{\text{PM}} \cdot \sin(\omega t). \tag{10}$$

The appearing phase shift $\gamma$ between $u_s(t)$ and $u_{\text{ind}}(t)$ (in case of field-oriented control, this angle appears between $u_s(t)$ and $i_s(t)$, too) was already defined in (4).

Fig. 12 shows the equivalent diagram of the whole motor drive [Fig. 12(a)], the equivalent circuit only with the stator voltage source $u_s(t)$ [Fig. 12(b)], and the circuit only

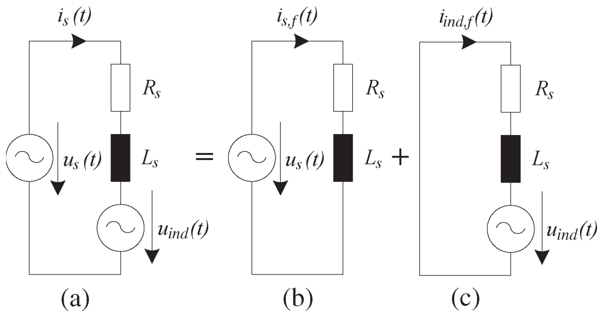


Fig. 12. Superposition of voltage sources appearing in a PMSM.

with the induced voltage $u_{\text{ind}}(t)$ [Fig. 12(c)]. One can see that the induced voltage $u_{\text{ind}}(t)$ is driving a fictitious current $i_{\text{ind},f}(t)$ [23]

$$i_{\text{ind},f}(t) = -\frac{\omega \Psi_{\text{PM}}}{\sqrt{R_s^2 + \omega^2 L_s^2}} \cdot \sin(\omega t - \tau_{\text{ind}}) \qquad (11)$$

which is part of the stator current $i_s(t)$ and can therefore be estimated out of $i_s(t)$ during the freewheeling state 2. The current $i_s(t)$ contains, therefore, information about $i_{\text{ind},f}(t)$, which on its part contains information about the actual rotor angle $\varphi$.

The fictitious current $i_{s,f}(t)$ before activating the freewheeling state is given by

$$i_{s,f}(t) = \frac{U_s}{\sqrt{R_s^2 + \omega^2 L_s^2}} \cdot \sin(\omega t + \gamma - \tau_s)\ \forall\, t < t_{\text{off}}. \qquad (12)$$

The phase shift $\tau_s$ appearing between the stator voltage $u_s(t)$ and $i_{s,f}(t)$ is equal to the phase shift $\tau_{\text{ind}}$ in (11) between the negative induced voltage $-u_{\text{ind}}(t)$ and the fictitious current $i_{\text{ind},f}(t)$ and can be written, in case of field-oriented control, as

$$\tau_s = \tau_{\text{ind}} = \arctan\left(\frac{\omega L_s}{R_s}\right). \qquad (13)$$

After turning off the stator voltage $u_s(t)$ ($t \geq t_{\text{off}}$ with $t_{\text{off}} = \varphi_{\text{off}}/\omega$), the fictitious stator current $i_{s,f}(t)$ decreases by an exponential function (cf. Fig. 11)

$$i_{s,f}(t) = i_{s,f}(t_{\text{off}}) \cdot e^{-(t-t_{\text{off}})\frac{R_s}{L_s}}\ \forall\, t > t_{\text{off}}. \qquad (14)$$

The current shunts (cf. Fig. 10) can be used to measure $i_s(t)$ during the turn-off window.

Near the zero crossing of $u_{\text{ind}}(t)$, the current $i_{\text{ind},f}(t)$ shows a peak, which also appears in $i_s(t)$ (cf. Fig. 11) with a phase shift of $\varphi_{i,s}$ caused by $i_{s,f}(t)$ [cf. (14)]. This appearing peak in $i_s(t)$ can be detected, and the actual angle of $u_{\text{ind}}(t)$, which is used for synchronization, is calculated as (cf. Fig. 11, derivation steps indicated with steps 1, 2, 3)

$$\varphi_{\text{sync}} = \underbrace{\varphi_{i,s}}_{\text{Step 1}} - \underbrace{90^\circ}_{\text{Step 2}} + \underbrace{\tau_{\text{ind}}}_{\text{Step 3}} \qquad (15)$$

by taking the phase shift $\varphi_{i,s}$, caused by the decay of $i_{s,f}(t)$, into account. As can be seen in Fig. 11, $\varphi_{\text{sync}}$ represents the time interval between the induced voltage zero crossing and the moment of peak detection and therefore is the actual rotor angle.

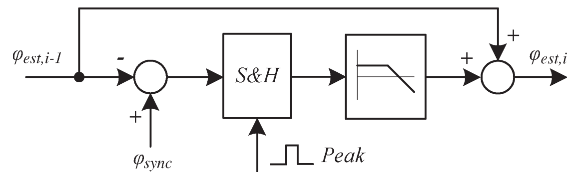


Fig. 13. Synchronization of the estimated rotor angle $\varphi_{\text{est}}$ through the calculated synchronization angle $\varphi_{\text{sync}}$.

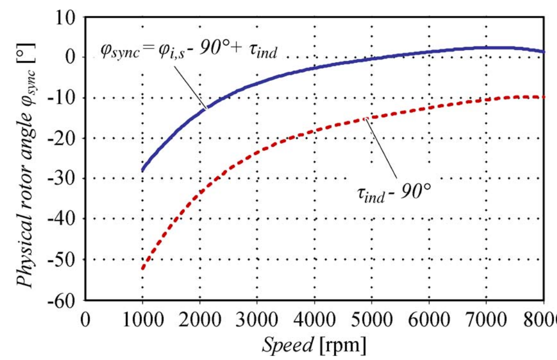


Fig. 14. Calculation of $\varphi_{\text{sync}}$ at the moment of peak detection for a fixed turn-off angle $\varphi_{\text{off}}$.

The synchronization block diagram is shown in Fig. 13. The detected peak in $i_s(t)$ activates the sample and hold block, and the difference between the estimated and the synchronization angle is low-pass filtered and added to the actual estimated rotor angle $\varphi_{\text{est},i-1}$. The low-pass filter is important, due to the necessity of a continuous angular signal for the operation of a PMSM.

The value of $\varphi_{\text{sync}}$ can be seen in Fig. 14 for a fixed turn-off angle $\varphi_{\text{off}}$. This correction can be calculated analytically by using (11), (13), and (14). However, the implementation of the calculation is not advisable on a digital signal processor, since the computational time and storage space are limited. Therefore, a lookup table should be generated for a practical implementation. The influence of the load [cf. (9) and (12)] on the decay of $i_{s,f}(t)$ can be considered in the analytical angle calculation and in the implemented lookup table, respectively. For reduced complexity, the turn-off angle $\varphi_{\text{off}}$ should be assumed to be constant with respect to $u_{\text{ind}}(t)$ to simplify the calculation of $i_{s,f}(t_{\text{off}})$ and, furthermore, the decay of $i_{s,f}(t)$.

Measurements of typical appearing waveforms are shown in Fig. 15. One can see that the estimated rotor angle $\varphi_{\text{est}}$ fits perfectly with the measured hall signal $\varphi_{\text{hall}}$. The lower lines show the measured voltage over $R_{\text{shunt}}$ representing the phase current and the detected peak signal produced by the implemented software. The peak in $i_s(t)$ during the freewheeling path can be seen directly.

As one can see, the introduced method is still depending on the machine parameters $L_s$ and $R_s$ [cf. (9) and (12)]. Therefore, the same performance concerning fluctuation of these parameters will be achieved as for the rotor-angle estimation. However, these motor parameters are usually well known or can be estimated [24], and the fluctuation is within a tolerable range. The main improvement of the synchronization method concerns

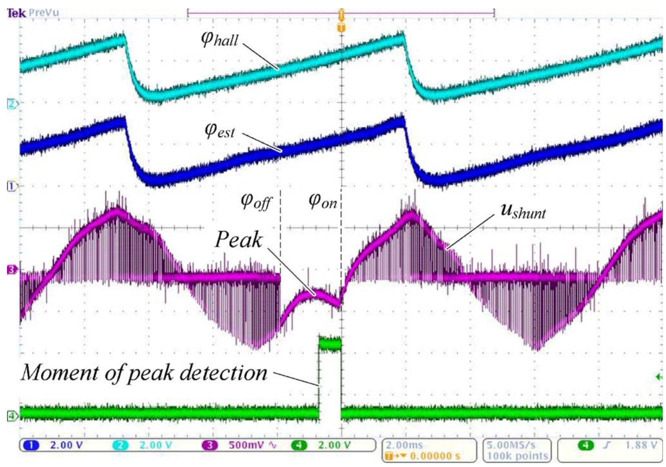


Fig. 15. Angle calculation at 7000 r/min in comparison to the measured angle at a hydraulic operation point of 6.5-L/min hydraulic flow and 1.3-bar outlet pressure and measured freewheeling current (angle scale: 240°/div for channels 1 and 2; voltage scale: 500 mV/div for channel 3 and 2 V/div for channel 4; and time scale: 2 ms/div).

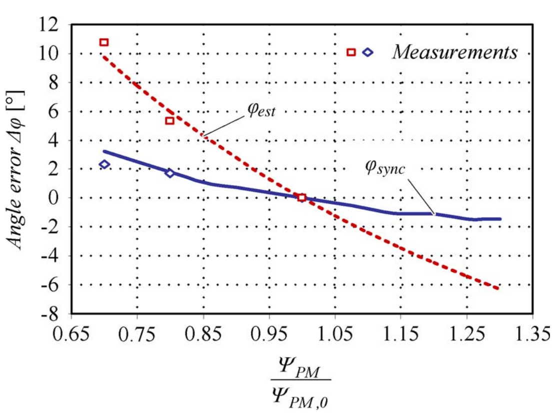


Fig. 16. Quality of the calculated rotor angle in dependence on permanent magnet flux variation (the magnetic flux degrading has been achieved through heating up the permanent magnet rotor according to Fig. 17).

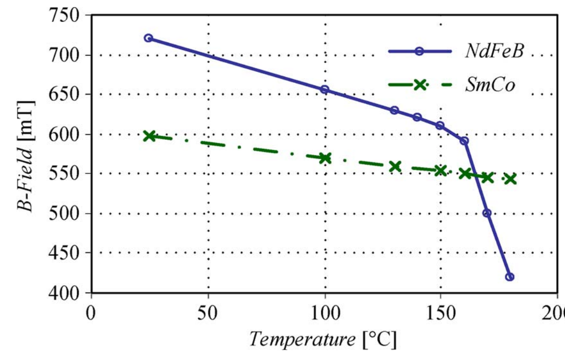


Fig. 17. Temperature dependence of *NdFeB* (*VACODYM 633HR*) and *SmCo* (*VACOMAX 225HR*) permanent magnets.

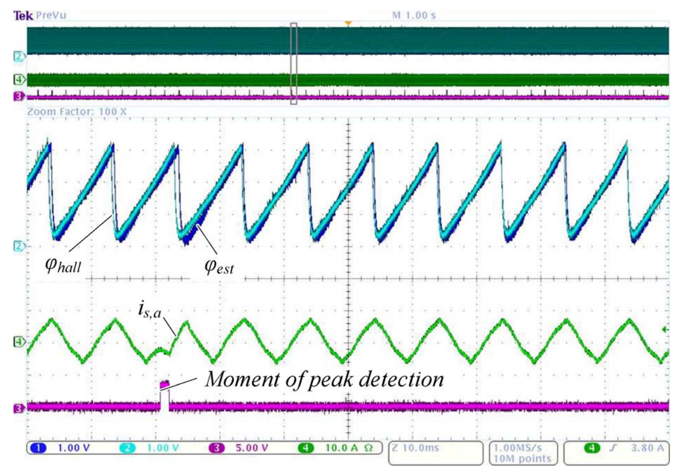


Fig. 18. Influence of synchronization on the wrong estimated angle $\varphi_{\mathrm{est}}$ due to a prior load change (angle scale: 120°/div; current scale: 10 A/div; voltage scale: 5 V/div; and time scale: 10 ms/div).

fluctuations of the rotor magnet field density. As shown in Fig. 16, the quality of the rotor-angle estimation is depending on the magnetic field impressed by the rotor $\Psi_{\mathrm{PM}}$ [cf. (4)], while in contrast, almost no dependence on the magnetic field for the method introduced in this section appears. Since a method for driving a magnetically levitated pump at high fluid temperatures has to be found and the magnetic flux $\Psi_{\mathrm{PM}}$ is highly depending on the fluid temperature (cf. Fig. 17), this influence is of high importance and must not be neglected. As shown in Fig. 17, the impressed magnetic flux will be decreased about 20%–30% for a fluid temperature increase of around 150 °C. As depicted in Fig. 16, this leads to a calculation error of $\varphi_{\mathrm{est}}$ up to 10°, whereas if the rotor angle is synchronized as presented in this section, the same magnetic field reduction leads to a calculation error of $\varphi_{\mathrm{sync}} = 2°$.

As mentioned before, also a system failure can be detected by synchronizing the estimated rotor angle $\varphi_{\mathrm{est}}$ with the introduced method in this section, as no peak in $i_s(t)$ will appear at standstill.

Since the introduced method turns off one drive phase for almost 1/4 period, a torque reduction may result. In [25, eq. (18)], the influence of repetitive nonsinusoidal currents on torque generation of bearingless motor drives has been calculated. Adapting this equation to the pump at hand shows that for operation in air above $n_{\min} = 1258$ r/min, no significant torque ripple occurs. Driving the pump with water will further decrease this calculated minimum needed speed significantly below 1000 r/min. In addition, the synchronization appears only in one phase and at one of 10–50 cycles; wherefore, the current distortion caused by turning off the phase voltage through this method does not have any influence on the pump operation.

## V. Improvement by Angle Synchronization

The improvement by synchronizing the estimated rotor angle $\varphi_{\mathrm{est}}$ according to the previous section can be seen in the measurements shown in Fig. 18. The estimated angle $\varphi_{\mathrm{est}}$ is calculated wrongly due to a prior load change until the synchronization is turned on and the angle is corrected. For the measurements done in this section, the same test setup as mentioned in Section III was used (cf. Fig. 9).

Fig. 19 shows the response of the system to a rotational speed reference step. As the zoom shows, this leads to a steady offset in the estimated rotor angle $\varphi_{\mathrm{est}}$ [cf. Fig. 19(a)] which cannot be detected by the estimation algorithm. By synchronizing the estimated angle $\varphi_{\mathrm{est}}$ with $\varphi_{\mathrm{sync}}$ as described before, the

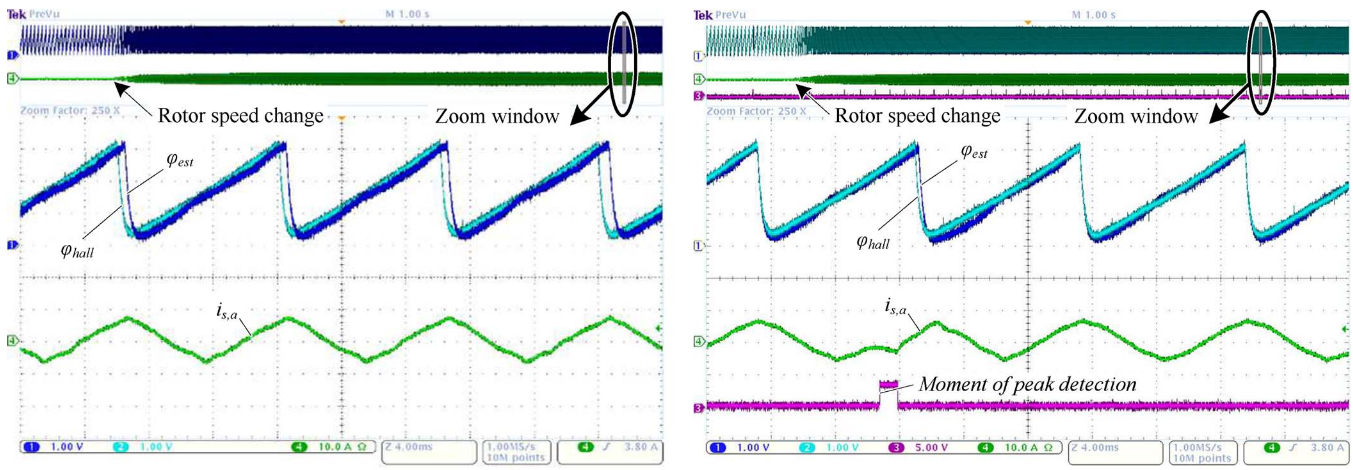


(a) (b)

Fig. 19. Rotor angle after a speed step from 1000 to 6000 r/min at full load (hydraulic flow: 14 L/min; hydraulic pressure: 0.7 bar). (a) A speed step leads to a permanent angle offset in case of angle estimation. (b) The appearing offset can be eliminated by angle synchronization (angle scale: 120°/div; current scale: 10 A/div; voltage scale: 5 V/div; and time scale: 4 ms/div).

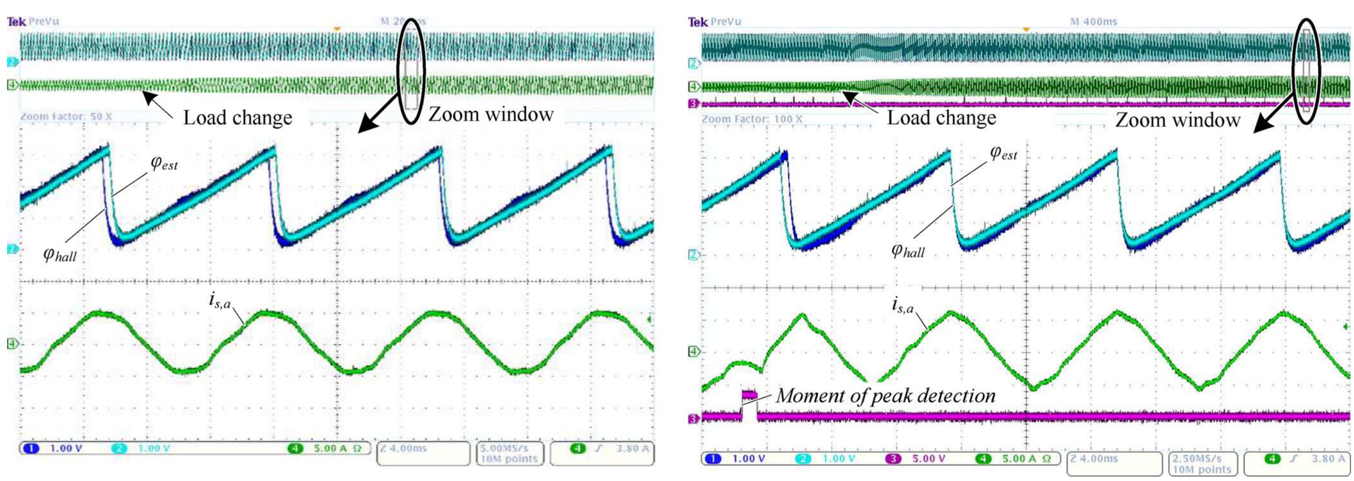


(a) (b)

Fig. 20. Rotor angle after a load step at 6000 r/min from zero load (hydraulic flow: 0 L/min; hydraulic pressure: 0.8 bar) to full load (hydraulic flow: 14 L/min; hydraulic pressure: 0.7 bar). (a) A load step leads to a permanent angle offset in case of angle estimation. (b) The appearing offset can be eliminated by angle synchronization (angle scale: 120°/div; current scale: 10 A/div; voltage scale: 5 V/div; and time scale: 4 ms/div).

constant offset can be eliminated [cf. Fig. 19(b)]. During the peak detection, a small offset appears, which results from turning off the angle estimation during this state. However, this error is eliminated permanently after one turn by the synchronization algorithm.

Finally, the angle calculation in case of a load step from zero load to full load is shown in Fig. 20. The resulting error after a step in the estimated angle $\varphi_{\mathrm{est}}$ is corrected through the synchronization and thus $\varphi_{\mathrm{sync}}$ in the same manner.

## VI. Conclusion

High fluid temperatures, as they are needed in semiconductor industry to further increase the process speed, cause problems for the bearingless pump system, since temperature-critical Hall sensors have to be placed close to the fluid to measure satisfying signals. This paper introduces a new control method of a PMSM bearingless pump by estimating and calculating the rotor angle without using temperature-critical Hall sensors.

First, the initial rotor angle is calculated using the radial position sensorics to enable levitation. This method uses an inherent property of unipolar permanent magnets, as always one pole is sticking to the stator wall. An algorithm was described to find out which pole is sticking to finally calculate the rotor angle and startup levitation.

Second, a simple but powerful method for estimating the actual rotor angle in a speed range of 1000–8000 r/min by using the impressed stator voltage and calculating the load-dependent phase shift between the stator voltage and the induced voltage is described. Measurements show that the estimated angle is equal to the measured rotor angle even at high load. However, this method is basically a feedforward control, and therefore, a synchronization with a discrete physical rotor-angle information is necessary to ensure a stable operation.

A method to calculate the actual physical angle out of the freewheeling current of one drive phase for synchronization with the estimated angle is described subsequently. This method greatly improves the robustness of the angle calculation against permanent magnet flux density degrading as it occurs for pump operations with high fluid temperatures. This improvement is finally verified by various measurements on an existing bearingless pump prototype system, e.g., for load steps and rotational speed steps.

With the described methods, an important step toward a hall-sensorless bearingless pump system for fluid temperatures beyond 150 °C is done by implementing a combination of all introduced methods.

## REFERENCES


[1] M. Neff, "Bearingless centrifugal pump for highly pure chemicals," in *Proc. 8th ISMB*, Aug. 2002, pp. 283–287.

[2] M. Neff, "Bearingless pump system for the semiconductor industry," in *Proc. 6th Int. Symp. Magn. Suspension Technol.*, 2001, pp. 169–173.

[3] N. Barletta, "Der lagerlose Scheibenläufer," Ph.D. dissertation, Elect. Eng. Design Lab., ETH Zürich, Zürich, Switzerland, 1998.

[4] J. Bichsel, "The bearingless electrical machine," in *Proc. Int. Symp. Magn. Suspension Technol.*, Aug. 19–23, 1991, vol. 2, pp. 1–14.

[5] T. Nussbaumer, K. Raggl, P. Boesch, and J. W. Kolar, "Trends in integration for magnetically levitated pump systems," in *Proc. PCC*, Nagoya, Japan, Feb. 2007, pp. 1551–1558.

[6] P. P. Acarnley and J. F. Watson, "Review of position-sensorless operation of brushless permanent-magnet machines," *IEEE Trans. Ind. Electron.*, vol. 53, no. 2, pp. 352–362, Apr. 2006.

[7] K.-Y. Lian, C.-H. Chiang, and H.-W. Tu, "LMI–based sensorless control of permanent-magnet synchronous motors," *IEEE Trans. Ind. Electron.*, vol. 54, no. 5, pp. 2769–2778, Oct. 2007.

[8] S.-Y. Kim and I.-J. Ha, "A new observer design method for HF signal injection sensorless control of IPMSMs," *IEEE Trans. Ind. Electron.*, vol. 55, no. 6, pp. 2525–2529, Jun. 2008.

[9] J.-S. Kim and S.-K. Sul, "New approach for high-performance PMSM drives without rotational position sensors," *IEEE Trans. Power Electron.*, vol. 12, no. 5, pp. 904–911, Sep. 1997.

[10] R. Wu and G. R. Slemon, "A permanent magnet motor drive without a shaft sensor," *IEEE Trans. Ind. Appl.*, vol. 27, no. 5, pp. 1005–1011, Sep./Oct. 1991.

[11] N. Matsui, T. Takeshita, and K. Yasuda, "A new sensorless drive of brushless DC motor," in *Proc. Int. Conf. Ind. Electron., Control, Instrum., Autom./Power Electron. Motion Control*, 1992, vol. 1, pp. 430–435.

[12] N. Matsui, "Sensorless PM brushless DC motor drives," *IEEE Trans. Ind. Electron.*, vol. 43, no. 2, pp. 300–308, Apr. 1996.

[13] N. Matsui and M. Shigyo, "Brushless DC motor control without position and speed sensors," *IEEE Trans. Ind. Appl.*, vol. 28, no. 1, pp. 120–127, Jan./Feb. 1992.

[14] Y.-H. Kim and Y.-S. Kook, "High performance IPMSM drives without rotational position sensors using reduced-order EKF," *IEEE Trans. Energy Convers.*, vol. 14, no. 4, pp. 868–873, Dec. 1999.

[15] P. Vas, *Sensorless Vector and Direct Torque Control*. London, U.K.: Oxford Univ. Press, 1998.

[16] M. Schrödl, "Sensorless control of permanent-magnet synchronous motors," *Elect. Power Compon. Syst.*, vol. 22, pp. 173–185, 1994.

[17] M. J. Corley and R. D. Lorenz, "Rotor position and velocity estimation for a salient-pole permanentmagnet synchronous machine at standstill and high speeds," *IEEE Trans. Ind. Appl.*, vol. 34, no. 4, pp. 784–789, Jul./Aug. 1998.

[18] A. B. Kulkarni and M. Ehsani, "A novel position sensor elimination technique for the interiorpermanent-magnet synchronous motor drive," *IEEE Trans. Ind. Appl.*, vol. 28, no. 1, pp. 144–150, Jan./Feb. 1992.

[19] K. Raggl, T. Nussbaumer, and J. W. Kolar, "Comparison of winding concepts for bearingless pumps," in *Proc. 7th ICPE*, Oct. 2007, pp. 1013–1020.

[20] T. Tera, Y. Yamauchi, A. Chiba, T. Fukao, and M. A. Rahman, "Performances of bearingless and sensorless induction motor drive based on mutual inductances and rotor displacements estimation," *IEEE Trans. Ind. Electron.*, vol. 53, no. 1, pp. 187–194, Feb. 2006.

[21] S. Burger, "Magnetgelagertes Pumpsystem für hohe Betriebstemperaturen," Ph.D. dissertation, Power Electron. Syst. Lab., ETH Zürich, Zürich, Switzerland, 2006.

[22] S. Bolognani, R. Oboe, and M. Zigliotto, "Sensorless full-digital PMSM drive with EKF estimation of speed and rotor position," *IEEE Trans. Ind. Electron.*, vol. 46, no. 1, pp. 184–191, Feb. 1999.

[23] R. Mizutani, T. Takeshita, and N. Matsui, "Current model-based sensorless drives of salient-pole PMSM at low speed and standstill," *IEEE Trans. Ind. Appl.*, vol. 34, no. 4, pp. 841–846, Jul./Aug. 1998.

[24] M. Rashed, P. F. A. MacConnel, A. F. Stronach, and P. Acarnley, "Sensorless indirect-rotor-field-orientation speed control of a permanent-magnet synchronous motor with stator-resistance estimation," *IEEE Trans. Ind. Electron.*, vol. 54, no. 3, pp. 1664–1675, Jun. 2007.

[25] M. T. Bartholet, T. Nussbaumer, D. Krähenbühl, F. Zürcher, and J. W. Kolar, "Modulation concepts for the control of a two-phase bearingless slice motor utilizing three-phase power modules," in *Proc. 4th PCC*, Apr. 2007, pp. 816–823.



**Klaus Raggl** (M'06) was born in Zams, Austria, in 1980. He received the M.Sc. degree in mechatronics from Johannes Kepler University Linz, Linz, Austria, in 2005, and the Ph.D. degree from the Power Electronic Systems Laboratory, Swiss Federal Institute of Technology (ETH), Zurich, Switzerland, in 2009. During his Ph.D. studies, he worked on bearingless pump systems with high power density in the Drive Technology and Magnetic Bearings Section.

Since April 2009, he has been with Hilti AG, Schaan, Liechtenstein, where he is currently working on high-performance drilling and demolition machines.



**Bernhard Warberger** was born in Zirl, Austria, in 1977. He received the M.S. degree in mechatronics from Johannes Kepler University Linz, Linz, Austria, in 2008.

Since April 2008, he has been with Levitronix GmbH, Zurich, Switzerland, where he is currently working on power supplies for magnetically levitated motors.



**Thomas Nussbaumer** (M'05) was born in Vienna, Austria, in 1975. He received the M.Sc. degree (with honors) in electrical engineering from Vienna University of Technology, Vienna, in 2001, and the Ph.D. degree from the Power Electronic Systems Laboratory, Swiss Federal Institute of Technology (ETH), Zurich, Switzerland, where he performed research on the design, control, and modulation of three-phase rectifiers with low effects on the mains, in 2004.

After receiving the Ph.D. degree, he continued his research on power factor correction techniques, modeling and dynamic control of three-phase rectifiers, and electromagnetic compatibility. Since February 2006, he has been with Levitronix GmbH, Zurich, where he is currently working on magnetically levitated motors and pumps for the semiconductor process industry.

**Simon Burger** was born in Aarau, Switzerland, in 1976. He received the Dipl.Ing.(electrical engineering) degree from the Swiss Federal Institute of Technology (ETH), Zurich, Switzerland, in 2002, and the Ph.D. degree from the Power Electronic Systems Laboratory (PES), ETH, in 2006.

During his Ph.D. studies, he was involved in research on magnetically levitated centrifugal pumps for high-temperature and high-purity semiconductor applications. Since June 2007, he has been with Speck Pumpen GmbH & Co. KG, Neunkirchen am Sand, Germany, where he is currently working on pumps, vacuum systems, and EC drives for special industry applications.

**Johann W. Kolar** (M'89–SM'04) received the Ph.D. degree (*summa cum laude/promotio sub auspiciis praesidentis rei publicae*) from the University of Technology Vienna, Austria.

Since 1984, he has been an Independent International Consultant in close collaboration with the Vienna University of Technology, in the fields of power electronics, industrial electronics, and high-performance drives. On February 1, 2001, he was appointed as a Professor and Head of the Power Electronic Systems Laboratory, Swiss Federal Institute of Technology (ETH), Zurich, Switzerland. He has proposed numerous novel PWM converter topologies, and modulation and control concepts, e.g., the VIENNA rectifier and the three-phase ac–ac sparse matrix converter. He has published over 300 scientific papers in international journals and conference proceedings. He is the holder of 75 patents. His current research is on ac–ac and ac–dc converter topologies with low effects on the mains, e.g., for power supply of telecommunication systems, more electric aircraft, and distributed power systems in connection with fuel cells. His other main areas of research include the realization of ultracompact intelligent converter modules employing latest power semiconductor technology (SiC), novel concepts for cooling and EMI filtering, multidomain/multiscale modeling and simulation, pulsed power, bearingless motors, and power MEMS.

Dr. Kolar is a member of the Institute of Electrical Engineers of Japan (IEEJ) and the technical program committees of numerous international conferences in the field (e.g., Director of the Power Quality Branch of the International Conference on Power Conversion and Intelligent Motion). From 1997 to 2000, he served as an Associate Editor of the IEEE TRANSACTIONS ON INDUSTRIAL ELECTRONICS, and since 2001, as an Associate Editor of the IEEE TRANSACTIONS ON POWER ELECTRONICS. Since 2002, he has been an Associate Editor for the *Journal of Power Electronics* of the Korean Institute of Power Electronics and a member of the Editorial Advisory Board of the IEEJ *Transactions on Electrical and Electronic Engineering*. He was the recipient of the Best Transactions Paper Award of the IEEE Industrial Electronics Society in 2005 and an Erskine Fellowship from the University of Canterbury, New Zealand, in 2003. In 2006, the European Power Supplies Manufacturers Association awarded the Power Electronics Systems Laboratory of ETH Zurich as the leading academic research institution in Europe.